Estimating the Wall Heat Flux of Unsteady Conjugated Forced Convection Between Two Corotating Disks Using an Inverse Solution Scheme

David T. W. Lin[1]
Associate Professor
Insitute of Engineering Technology,
National University of Tainan,
Tainan City 700, Taiwan, R.O.C.
e-mail: david@mail.nutn.edu.tw

Hung Yi Li

Wei Mon Yan

Department of Mechatronic Engineering,
Huafan University,
Shih Ting, Taipei 223, Taiwan, R.O.C.

An inverse solution scheme based on the conjugate gradient method with the minimization of the object function is presented for estimating the unknown wall heat flux of conjugated forced convection flows between two corotating disks from temperature measurements acquired within the flow field. The validity of the proposed approach is demonstrated via the estimation of three time- and space-dependent heat flux profiles. A good agreement is observed between the estimated results and the exact solution in every case. In general, the accuracy of the estimated results is found to improve as the temperature sensors are moved closer to the unknown boundary surface and the error in the measured temperature data is reduced. [DOI: 10.1115/1.2976788]

Keywords: inverse solution, conjugated forced convection, conjugate gradient method, corotating disks

1 Introduction

The problem of fluid flow and heat transfer in radial flows between two corotating disks is of practical significance in many engineering applications. In many cases, the fluid flow and heat transfer characteristics are unsteady. However, in conjugated heat transfer problems involving corotating disks, it is frequently difficult, if not impossible, to measure the heat flux or temperature at the rotating disk surface. Therefore, the use of some form of inverse technique is generally required. However, such inverse problems are ill-posed, and hence the estimated solutions are highly sensitive to errors in the measured input data. Various researchers have proposed methods for overcoming the inherent instability of inverse solution schemes [1–4].

Moutsoglou [5] considered the problem of steady-state forced convection between parallel flat plates and used a straight inversion scheme and the whole domain regularization technique to estimate the unknown heat flux at the upper plate surface from temperature data measured at the lower plate. Colaco and Orlande [6] investigated the inverse problem of predicting two boundary heat fluxes in irregularly shaped channels containing a forced convection flow. Huang and Ozisik [7] determined the spacewise variation of the heat flux along a parallel plate duct containing a laminar flow stream from temperature measurements acquired at various locations within the flow field. Liu and Ozisik [8] employed the conjugate gradient method and an adjoint equation to conduct an inverse analysis of the timewise variation of the wall heat flux for the case of transient turbulent forced convection within a parallel plate duct. Raghunath [9], Bokar and Ozisik [10], and Liu and Ozisik [11] considered the inverse convection problem of determining the inlet temperature of a thermally developing hydrodynamically developed laminar flow between parallel plates from temperature measurements taken downstream of the entrance region. Machado and Orlande [12] applied the conjugate gradient method with an adjoint equation to estimate the timewise and spacewise variations of the wall heat flux of a parallel plate channel containing a laminar forced convection flow. Park and Lee [13] derived the space-dependent wall heat flux of a duct containing laminar flow using the Karhunen–Loeve Galerkin procedure. Fic [14] presented an inverse solution scheme for estimating the boundary velocity in steady-state convection-diffusion heat transfer problems with a potential fluid flow. Li and Yan considered the inverse problem of estimating the space- and time-dependent wall heat flux distributions for an unsteady forced convection within a parallel plate duct [15,16] and an annular duct [17], respectively. In a more recent study, Chen et al. [18,19] considered the equivalent problem in a parallel annular duct.

Due to their practical significance, the fluid flow and heat transfer characteristics of flow systems involving rotating bodies have attracted considerable attention. For example, Attia [20] considered the unsteady flow of an incompressible viscous non-Newtonian fluid above an infinite rotating disk. Seghir-Ouali et al. [21] employed an experimental approach to investigate the problem of convective heat transfer within a rotating cylinder with an axial air flow. Siddiqui et al. [22] obtained numerical solutions for the effects of the hall current and heat transfer on the magnetohydrodynamic (MHD) flow of a Burger's fluid induced by the pull of eccentric rotating disks. Aus der Wiesche [23] performed large-eddy simulations to establish the heat transfer characteristics of a pair of corotating disks in a parallel air crossflow.

In unsteady conjugated heat transfer problems, the heat capacity of the wall has a significant effect on the transient characteristics of the forced convection heat transfer performance. The effects of wall conduction on the characteristics of mixed convection channel flows in the direct solver were studied by Lee and Yan [24] and Yan and Lee [25], and the results indicated that both the conduction in the wall and the wall heat capacity play an important role in unsteady conjugated mixed convection channel flow. Yan and Lee [26] also examined the characteristics of unsteady conjugated mixed convection flow and the heat transfer between two corotating disks. In Ref. [27], Luna et al. applied the energy equation and the integral boundary layer technique to per-

[1]Corresponding author.

Contributed by the Heat Transfer Division of ASME for publication in the JOURNAL OF HEAT TRANSFER. Manuscript received October 24, 2007; final manuscript received April 21, 2008; published online September 24, 2008. Review conducted by Peter Vadasz.

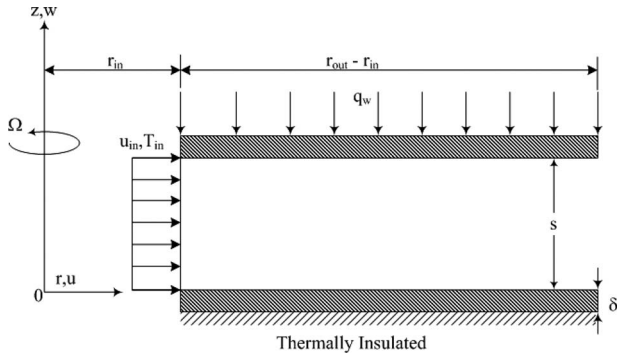

Fig. 1 Geometry and coordinate system

form a transient analysis of the conjugated heat transfer process in the thermal entrance region of a circular duct containing a fully developed laminar power-law fluid flow. Indinger and Shevchuk [28] presented numerical solutions for the transient laminar heat transfer characteristics of a rotating disk heated to a constant temperature and then suddenly subjected to unsteady cooling in still air. Ozar et al. [29] and Basu and Cetegen [30,31] observed heat transfer phenomena in a thin liquid film flowing over a rotating disk by the experiment and numerical method, separately. In a later study, Shevchuk [32] examined the unsteady conjugated heat transfer problem of a nonuniformly heated rotating disk. Lallave et al. [33] investigated the conjugate heat transfer characteristics of a rotating uniformly heated solid disk of finite thickness and radius under the impingement of a confined liquid jet. Although the conjugated mixed convection problem with the rotating system was the concern of those previous researchers, the direct solution was used in most of these studies. Sladek et al. [34] combined the Stehfest algorithm, the Laplace inversion, and the meshless local Petrov–Galerkin method to solve the inverse heat conduction problem of fluid flows within 3-D axisymmetric rotating bodies.

Reviewing literature, it is found that the problem of the unsteady forced convection flow between two corotating disks has received relatively little attention. However, the heat transfer characteristics of radial flows between corotating disks are of practical significance in many engineering applications and therefore merit a detailed investigation. In general, most previous studies of conjugated mixed convection in rotating systems employed direct numerical approaches. However, in such systems, it is generally impractical to measure the heat flux or temperature at the rotating surface, and hence some form of inverse technique is required. Accordingly, the current study develops an inverse scheme to investigate the heat transfer characteristics of the unsteady laminar forced convection flow between two corotating disks. In the proposed approach, a conjugate gradient method is used to estimate the space- and time-dependent wall heat fluxes acting on the surface of the upper disk from temperature data acquired from various locations within the flow field.

2 Analysis

2.1 Direct Problem. Figure 1 presents a schematic of the problem considered in the present analysis. As shown, the parallel disks corotate at an angular speed Ω and have an opening of $2r_{\text{in}}$ at the center, a wall thickness of δ, and a separation of s. The geometry of the rotating disks is described using a cylindrical coordinate system (r,z). The inlet coolant fluid flows radially outwards through the annular space between the two disks at a uniform velocity u_{in} and a uniform temperature T_{in}. Initially, the entire system, i.e., the flowing fluid and the two disk walls, have a uniform temperature T_{in}. However, at time $t=0$, the upper disk wall is subjected to a wall heat flux q_w, which varies as a function of the time, t, or as a function of both the time and the radial position, r. As shown, the lower disk wall is thermally insulated.

The aim of the current inverse analysis is to estimate the heat flux profile along the surface of the upper disk based on temperature measurements acquired at different locations within the coolant fluid flow. To simplify the analysis, the following assumptions are made. (1) The flow is steady, incompressible, and axisymmetric. (2) The fluid is laminar and is a boundary layer flow. (3) The flow has a high Peclet number and thus conduction in the radial direction of the fluid is negligible. (4) The heat conducted in the radial direction of the wall is sufficiently small to be neglected. The following dimensionless quantities are introduced to nondimensionalize the governing equations:

$$R=\frac{r}{s},\quad Z=\frac{z}{s},\quad R_{\text{in}}=\frac{r_{\text{in}}}{s},\quad R'=R-R_{\text{in}},\quad \theta(R,Z,\tau)=\frac{T-T_{\text{in}}}{\Delta T_c}$$

$$\text{Pe}=\frac{u_{\text{in}}s}{\alpha_f},\quad \text{Re}=\frac{u_{\text{in}}}{s\nu},\quad \text{Ro}=\frac{\Omega s}{u_{\text{in}}},\quad Q=\frac{q_w}{q_{\text{ref}}}$$

$$U=\frac{u}{u_{\text{in}}},\quad V=\frac{v}{u_{\text{in}}},\quad W=\frac{w}{u_{\text{in}}},\quad P'=\frac{p'}{(\rho u_{\text{in}}^2)} \tag{1}$$

$$\tau=\frac{\alpha f^t}{s^2},\quad K=\frac{k_w}{k_f},\quad \lambda=\frac{\delta}{s},\quad A=\frac{\alpha_w}{\alpha_f}$$

where k_w and k_f are the thermal conductivities of the plate and the fluid, respectively, α_w and α_f are the thermal diffusivities of the plate and the fluid, separately, T is the temperature, q_w is the heat flux applied to the wall, and q_{ref} is the reference heat flux. In this paper, the heat transfer to the wall is assumed positive.

The dimensionless governing equations describing the problem shown in Fig. 1 have the following form.

For the continuity equation,

$$\frac{\partial(RU)}{\partial R}+R\frac{\partial W}{\partial Z}=0 \tag{2a}$$

For the radial momentum equation,

$$U\frac{\partial U}{\partial R}+W\frac{\partial U}{\partial Z}-\frac{V^2}{R}=-\frac{dP'}{dR}+\left(\frac{1}{\text{Re}}\right)\frac{\partial^2 U}{\partial Z^2}+2\text{Ro}V \tag{2b}$$

For the tangential momentum equation,

$$U\frac{\partial V}{\partial R}+W\frac{\partial V}{\partial Z}+\frac{UV}{R}=\left(\frac{1}{\text{Re}}\right)\frac{\partial^2 V}{\partial Z^2}-2\text{Ro}U \tag{2c}$$

For the energy equation,

$$\text{Fluid}\quad \left(\frac{1}{\text{Pe}}\right)\frac{\partial\theta_f}{\partial\tau}+U\frac{\partial\theta_f}{\partial R}+W\frac{\partial\theta_f}{\partial Z}=\left(\frac{1}{\text{Pe}}\right)\frac{\partial^2\theta_f}{\partial Z^2} \tag{2d}$$

$$\text{Plate}\quad \frac{\partial\theta_w}{\partial\tau}=A\frac{\partial^2\theta_w}{\partial Z^2} \tag{2e}$$

The corresponding initial conditions and boundary conditions are as follows:

$$\tau=0:\quad \theta_f=\theta_w=0 \tag{2f}$$

$$\tau>0:\quad R=R_{\text{in}}:\quad U-1=V=W=0,\quad \theta_f=\theta_w=0 \tag{2g}$$

$$Z=-\lambda:\quad \frac{\partial\theta_w(R,-\lambda,\tau)}{\partial Z}=0 \tag{2h}$$

$$Z=0:\quad U=V=W=0,\quad \theta_f=\theta_w,\quad K\frac{\partial\theta_w(R,0,\tau)}{\partial Z}=\frac{\partial\theta_f(R,0,\tau)}{\partial Z} \tag{2i}$$

$$Z=1: \quad U=V=W=0, \quad \theta_f=\theta_w, \quad K\frac{\partial\theta_w(R,1,\tau)}{\partial Z}=\frac{\partial\theta_f(R,1,\tau)}{\partial Z} \tag{2j}$$

$$Z=1+\lambda: \quad K\frac{\partial\theta_w(R,1+\lambda,\tau)}{\partial Z}=Q(R,\tau) \tag{2k}$$

In the direct problem, the heat flux applied to the surface of the upper disk is known, and the objective is to compute the dimensionless temperature distribution in the fluid flow between the two disks. In the direct solution procedure, the governing equations are transformed into finite difference equations using a fully implicit numerical scheme in which the r-direction convection term is approximated by the upstream difference method, the z-direction diffusion term by the central difference scheme, and the unsteady term by the backward difference scheme. Note that the full details of the numerical procedure are presented in Ref. [35] and are therefore omitted here. The resulting system of equations forms a tridiagonal matrix, which can then be solved using the Thomas algorithm [36].

2.2 Inverse Problem. In the direct problem described above, the velocity distribution, initial conditions, and boundary conditions are all known, and thus the temperature distribution in the flow field and the upper disk is easily derived. However, in the inverse problem, the dimensionless heat flux $Q(R,\tau)$ acting on the surface of the upper disk is not known and must be estimated from temperature data acquired using sensors located within the fluid stream. Essentially, the problem of estimating the wall heat flux from the measured temperature data involves minimizing the following objective function:

$$J=\sum_{i=1}^{M}\sum_{k=1}^{N}(\theta_{f,i,k}-\Theta_{i,k})^2 \tag{3}$$

where $\theta_{f,i,k}=\theta_f(R_i,Z_1,\tau_k)$ is the calculated dimensionless temperature corresponding to an estimated $Q(R,\tau)$ and $\Theta_{i,k}=\Theta(R_i,Z_1,\tau_k)$ is the measured dimensionless temperature. Note that $Z_1=0$ indicates that the temperature sensors are located at the interface between the fluid and the lower disk wall. Similarly, $0<Z_1<1$ implies that the sensors are positioned at some vertical height within the fluid stream, while $Z_1=1$ indicates that the temperature measurements are acquired at the interface between the fluid and the upper disk wall. Finally, M and N indicate the number of measurement data in the R and τ dimensions, respectively.

In the inverse solution procedure performed in this study, the conjugate gradient method [37] is used to determine the unknown wall heat flux $Q(R,\tau)$ by minimizing the objective function J. The iterative process employed to do so can be expressed as

$$Q_{m,n}^{p+1}=Q_{m,n}^{p}-\beta^p d_{m,n}^{p} \tag{4}$$

where $Q_{m,n}=Q(R_m,\tau_n)$, β^p is the step size, and $d_{m,n}^{p}$ is the direction of descent and is determined from

$$d_{m,n}^{p}=\left(\frac{\partial J}{\partial Q_{m,n}}\right)^p+\gamma^p d_{m,n}^{p-1} \tag{5}$$

in which the conjugate coefficient γ^p is calculated as

$$\gamma^p=\frac{\sum_{m=1}^{M}\sum_{n=1}^{N}\left[\left(\frac{\partial J}{\partial Q_{m,n}}\right)^p\right]^2}{\sum_{m=1}^{M}\sum_{n=1}^{N}\left[\left(\frac{\partial J}{\partial Q_{m,n}}\right)^{p-1}\right]^2} \quad \text{with} \quad \gamma^0=0 \tag{6}$$

In Eq. (6), $\partial J/\partial Q_{m,n}$ represents the gradient of the objective function. The step size β^p in Eq. (4) is determined from

$$\beta^p=\frac{\sum_{i=1}^{M}\sum_{k=1}^{N}(\theta_{f,i,k}^{p}-\Theta_{i,k})\sum_{m=1}^{M}\sum_{n=1}^{N}\left(\frac{\partial\theta_{f,i,k}}{\partial Q_{m,n}}\right)^p d_{m,n}^{p}}{\sum_{i=1}^{M}\sum_{k=1}^{N}\left[\sum_{m=1}^{M}\sum_{n=1}^{N}\left(\frac{\partial\theta_{f,i,k}}{\partial Q_{m,n}}\right)^p d_{m,n}^{p}\right]^2} \tag{7}$$

where $\partial\theta_{f,i,k}/\partial Q_{m,n}$ is the sensitivity coefficient. This coefficient can be obtained by differentiating the direct problem with respect to $Q_{m,n}$, i.e.,

$$\left(\frac{1}{\mathrm{Pe}}\right)\frac{\partial}{\partial\tau}\left(\frac{\partial\theta_f}{\partial Q_{m,n}}\right)+U\frac{\partial}{\partial R}\left(\frac{\partial\theta_f}{\partial Q_{m,n}}\right)+W\frac{\partial}{\partial Z}\left(\frac{\partial\theta_f}{\partial Q_{m,n}}\right)=\left(\frac{1}{\mathrm{Pe}}\right)\frac{\partial^2}{\partial Z^2}\left(\frac{\partial\theta_f}{\partial Q_{m,n}}\right) \tag{8a}$$

$$\frac{\partial}{\partial\tau}\left(\frac{\partial\theta_w}{\partial Q_{m,n}}\right)=A\frac{\partial^2}{\partial Z^2}\left(\frac{\partial\theta_w}{\partial Q_{m,n}}\right) \tag{8b}$$

$$\tau=0: \quad \frac{\partial\theta_f(R,Z,0)}{\partial Q_{m,n}}=\frac{\partial\theta_w(R,Z,0)}{\partial Q_{m,n}}=0 \tag{8c}$$

$$\tau>0: \quad R=R_{\mathrm{in}}: \quad \frac{\partial\theta_f(R_{\mathrm{in}},Z,\tau)}{\partial Q_{m,n}}=\frac{\partial\theta_w(R_{\mathrm{in}},Z,\tau)}{\partial Q_{m,n}}=0 \tag{8d}$$

$$Z=-\lambda: \quad \frac{\partial}{\partial Z}\left(\frac{\partial\theta_w(R,-\lambda,\tau)}{\partial Q_{m,n}}\right)=0 \tag{8e}$$

$$Z=0: \quad \frac{\partial\theta_f(R,0,\tau)}{\partial Q_{m,n}}=\frac{\partial\theta_w(R,0,\tau)}{\partial Q_{m,n}}=0 \tag{8f}$$

$$K\frac{\partial}{\partial Z}\left(\frac{\partial\theta_w(R,0,\tau)}{\partial Q_{m,n}}\right)=\frac{\partial}{\partial Z}\left(\frac{\partial\theta_f(R,0,\tau)}{\partial Q_{m,n}}\right) \tag{8g}$$

$$Z=1: \quad \frac{\partial\theta_f(R,1,\tau)}{\partial Q_{m,n}}=\frac{\partial\theta_w(R,1,\tau)}{\partial Q_{m,n}}=0 \tag{8h}$$

$$K\frac{\partial}{\partial Z}\left(\frac{\partial\theta_w(R,1,\tau)}{\partial Q_{m,n}}\right)=\frac{\partial}{\partial Z}\left(\frac{\partial\theta_f(R,1,\tau)}{\partial Q_{m,n}}\right) \tag{8i}$$

$$Z=1+\lambda: \quad K\frac{\partial}{\partial Z}\left(\frac{\partial\theta_w(R,1+\lambda,\tau)}{\partial Q_{m,n}}\right)=\hat{u}(R-R_m,\tau-\tau_n) \tag{8j}$$

for $m=1,2,\ldots,M$ and $n=1,2,\ldots,N$, where

$$\hat{u}(R-R_m,\tau-\tau_n)=\begin{cases}1 & \text{if } R=R_m, \quad \tau=\tau_n\\ 0 & \text{otherwise}\end{cases} \tag{8k}$$

The gradient of the objective function, $\partial J/\partial Q_{m,n}$, is determined by differentiating Eq. (3) with respect to $Q_{m,n}$, i.e.,

$$\frac{\partial J}{\partial Q_{m,n}}=2\sum_{i=1}^{M}\sum_{k=1}^{N}(\theta_{i,k}-\Theta_{i,k})\frac{\partial\theta_{f,i,k}}{\partial Q_{m,n}} \tag{9}$$

In general, if the inverse problem contains no measurement errors, the condition

$$J(Q_{m,n}^{p})<\varphi \tag{10}$$

can be used as a termination criterion for the iterative process, where φ is a small specified positive number. However, in the current case, the measured temperature data inevitably contain a degree of error. Accordingly, the termination criterion is specified using the discrepancy principle [38], i.e.,

$$J(Q_{m,n}^{p})<MN\sigma^2 \tag{11}$$

where σ is the standard deviation of the measurement error.

The computational procedure employed to solve the current inverse convection problem can be summarized as follows.

Step 1. Solve the sensitivity problem to calculate the sensitivity coefficient $\partial\theta_{f,i,k}/\partial Q_{m,n}$.

Step 2. Make an initial guess of the dimensionless heat flux $Q^0_{m,n}$ and set the iteration step number to $p=0$.

Step 3. Solve the direct problem to compute $\theta_{f,i,k}$.

Step 4. Calculate the objective function. Terminate the iteration process if the specified criterion is satisfied; otherwise go to Step 5.

Step 5. Knowing $\partial\theta_{f,i,k}/\partial Q_{m,n}$, $\theta_{f,i,k}$, and $\Theta_{i,k}$, compute the gradient of the objective function, $\partial J/\partial Q_{m,n}$.

Step 6. Knowing $\partial J/\partial Q_{m,n}$, compute γ^p and $d^p_{m,n}$.

Step 7. Knowing $\partial\theta_{f,i,k}/\partial Q_{m,n}$, $\theta_{f,i,k}$, $\Theta_{i,k}$, and $d^p_{m,n}$, compute for β^p.

Step 8. Knowing β^p and $d^p_{m,n}$, compute $Q^{p+1}_{m,n}$. Set $p=p+1$ and return to Step 3.

3 Results and Discussions

As described above, the aim of the current inverse analysis is to estimate the unknown heat flux acting on the surface of the upper disk in the corotating pair from temperature measurements taken within the flow field or at the interface between the flow field and the upper or lower disks. As shown in Fig. 1, three types of boundary are applied on the corotating disks, i.e., the interface between the disk wall and the fluid, the quantity of the heat flux entering the upper disk surface, and the adiabatic boundary on the lower disk wall. In practice, such temperature measurements inevitably contain a certain degree of error. To reflect this, the temperature data, Θ, used in the present simulations as the basis for estimating the unknown boundary conditions, are computed by adding a random error to the exact temperature solutions, θ, obtained by solving the direct problem, i.e.,

$$\Theta = \theta + \sigma\zeta \tag{12}$$

where σ is the standard deviation of the measurement data and ζ is a random variable with a normal distribution, a zero mean, and a unit standard deviation. The value of ζ is calculated using the IMSL subroutine DRNNOR [39] and is specified within the range $-2.576<\zeta<2.576$, which represents the 99% confidence bound for the measured temperature.

The validity and applicability of the proposed inverse solution procedure are demonstrated by considering three different heat flux profiles.

In Case 1,

$$Q(\tau) = 0.01\tau, \quad \tau \leq 500 \tag{13a}$$

$$Q(\tau) = 0.01(1000-\tau), \quad \tau > 500 \tag{13b}$$

In Case 2,

$$Q(\tau) = 5\ \sin(\pi\tau/1000) \tag{13c}$$

In Case 3,

$$Q(R,\tau) = 0.125R'\ \sin(\pi\tau/1000) \tag{13d}$$

As can be seen, the heat flux profiles in Cases 1 and 2 have the form of simple time-dependent triangular and sinusoidal functions, respectively, whereas Case 3 considers the rather more complicated scenario of a wall heat flux that varies both in time and space. In performing the simulations, the dimensionless thickness of the disk wall, λ, is assumed to be 0.1, and 41 equally spaced measurements are taken in the ranges $0\leq R'\leq 40$ and $0\leq\tau\leq 1000$, respectively. These data are then used as input data to reconstruct the unknown wall heat flux in the inverse problem. The simulations consider an air stream (Pr=0.7) flowing between two corotating disks with carbon steel walls ($K=2000$ and $A=0.65$). The opening radius, R_{in}, and the through-flow Reynolds number, Re, are assumed to be 20 and 500, respectively.

To evaluate the robustness of the proposed inverse solution procedure, the three heat flux profiles described in Eqs. (13*a*)–(13*d*) are estimated under the assumptions of measurement errors of $\sigma=0$, 0.03, 0.06, or 0.09, respectively, and sensor positions of $Z_1=0-0.9$. The accuracy of the estimated results is quantified using the following absolute average error index:

$$\varepsilon = \frac{1}{n_t}\sum_{j=1}^{n_t}|f-f_0| \tag{14}$$

where f is the estimated result with measurement errors, f_0 is the exact result, and n_t is the number of temporal steps. Clearly, a smaller value of ε indicates a better estimation result, and vice versa.

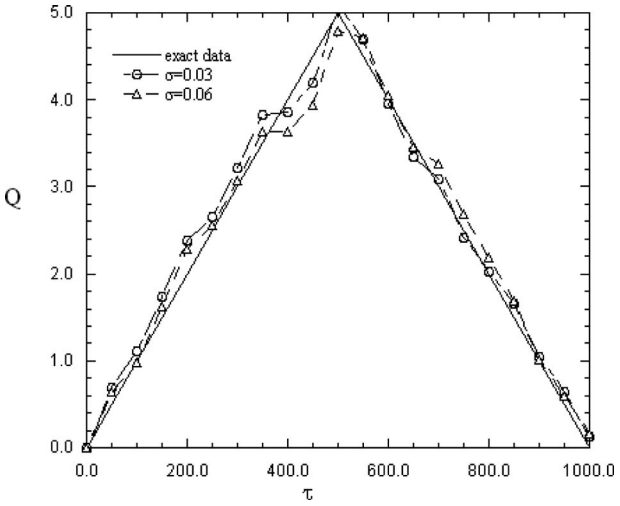

Fig. 2 Comparison of the exact result and inverse results ($\sigma=0.03$ and $\sigma=0.06$) for the Case 1 heat flux profile ($Z_1=0.9$)

Figure 2 compares the exact solution of the Case 1 heat flux profile with the estimated results obtained under the assumption of temperature measurement errors of $\sigma=0.03$ and $\sigma=0.06$, respectively. Note that in both cases, the temperature sensor is assumed to be located at $Z_1=0.9$. In general, when the temperature measurements are error-free, the estimated heat flux profile virtually coincides with the exact solutions. Furthermore, a good general agreement exists between the exact result and the inverse solutions even when the temperature measurements include an error component. Thus, the robustness of the proposed inverse solution scheme is confirmed. From inspection, the absolute average errors of the estimated dimensionless heat fluxes are found to be 0.144 and 0.174 for measurement errors of $\sigma=0.03$ and $\sigma=0.06$, respectively. In addition, the corresponding relative errors are computed to be around 2.88% and 3.48%, respectively, where the relative error is defined as the absolute average error divided by the maximum wall heat flux.

Figure 3(*a*) illustrates the variation of the absolute average error of the estimated results with the temperature measurement error as a function of the sensor location under various conditions in which σ ranges from 0.0 to 0.09 at $Z_1=0.0$, 0.3, 0.6, or 0.9, separately. In general, large measuring errors make the estimated results diverge from the error-free solutions. It is observed that the absolute average error increases with an increasing measurement error, but decreases with an increasing value of Z_1, i.e., the sensors are moved closer toward the upper disk. For convenience, the data presented in Fig. 3(*a*) are also tabulated in Table 1. It is noted in Table 1 that the absolute average errors are relatively amplified when σ is increased from 0.03 to 0.06, compared with that when σ is changed from 0.06 to 0.09, especially $Z_1=0.0$ and 0.3. From inspection, it is found that the absolute average error is highly sensitive to input data errors over the range $\sigma=0.03-0.06$, particularly when the sensors are located further from the unknown boundary surface, i.e., at $Z_1=0.0$ or $Z_1=0.3$, respectively. Figure

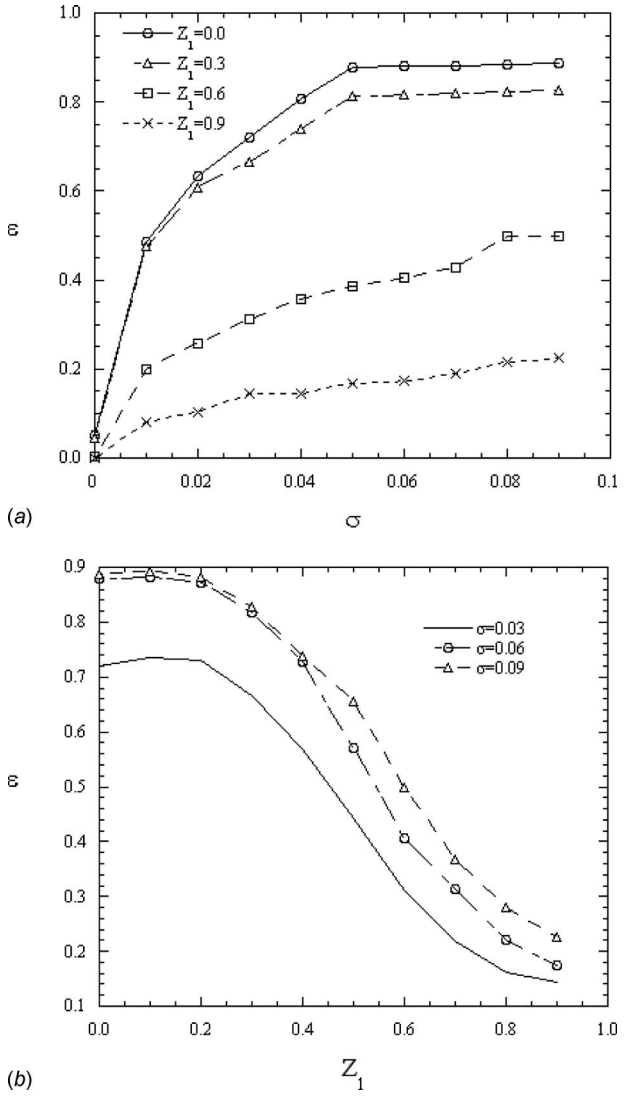

Fig. 3 Variation of the absolute average error with the (*a*) measurement error as a function of sensor location and (*b*) the sensor location as a function of the measurement error for the Case 1 heat flux profile

3(*b*) illustrates the variation of the absolute average error with the sensor location as a function of the temperature measurement error. It is apparent that irrespective of the magnitude of the measurement error, the absolute average error reduces significantly as the value of Z_1 increases beyond 0.2. In other words, an improved estimation performance is obtained as the sensors are moved closer to the unknown boundary of interest. Overall, the results show that the accuracy of the inverse solution scheme improves as the error in the temperature measurement data decreases or the distance between the temperature sensors and the upper boundary surface reduces.

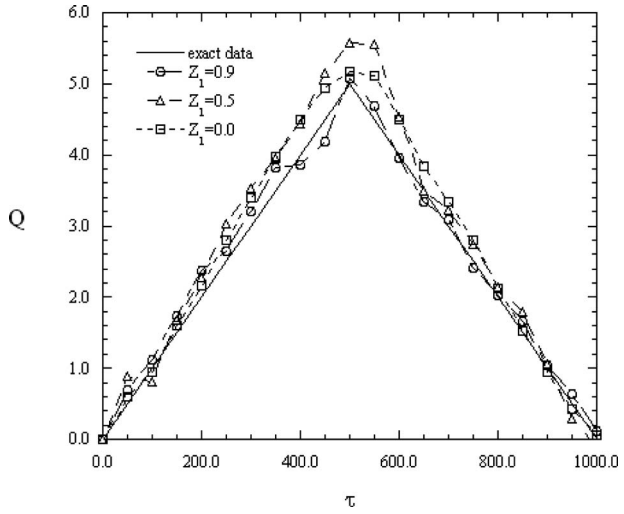

Fig. 4 Comparison of the exact result and inverse results (σ =0.03) for the Case 1 heat flux profile as a function of the sensor location

To evaluate the effect of the sensor location on the estimation performance of the proposed scheme, Fig. 4 compares the estimated and exact solutions for the Case 1 heat flux profile for a constant temperature measurement error of σ=0.03 and sensor locations of Z_1=0.0, 0.5, and 0.9, respectively. In general, it is seen that the deviation between the estimated results and the exact solution increases as the value of Z_1 decreases. In other words, the accuracy of the estimated heat flux reduces as the sensors are moved further from the unknown boundary surface.

To verify the applicability of the inverse solution scheme to the estimation of unknown time-dependent heat flux profiles of various forms, the simulation procedure described above was repeated for the second heat flux boundary condition, i.e., the time-dependent sinusoidal profile given in Eq. (13*c*). Figure 5(*a*) compares the exact solution with the estimated results obtained using input data with measurement errors of σ=0.03 and σ=0.06, respectively, and the sensor location is Z_1=0.9. As in Fig. 2, it can be seen that a good agreement is obtained between the exact result and the estimated solutions as the value of the measurement error is reduced. Figure 5(*b*) shows the effect of the sensor location on the accuracy of the estimated results given a constant measurement error of σ=0.03. As in the previous example, the deviation between the estimated result and the exact solution increases as the sensor is moved further from the upper wall. Figure 6 plots the variation of the absolute average error with the sensor location as a function of the measurement error. It is evident that the accuracy of the estimated results improves as the error in the measurement data decreases or the sensor is moved closer to the upper wall surface.

Finally, the wall heating condition of Case 3, which is a function of space (R') and time (τ), is tested. Figure 7 shows the estimated heat fluxes at R'=8, 20, and 32 under different measurement errors (σ=0.03 and σ=0.06) for wall heating conditions

Table 1 The absolute average errors at different σ and Z_1 for the wall heating condition of Case 1

σ	0.0	0.01	0.02	0.03	0.04	0.05	0.06	0.07	0.08	0.09
Z_1=0.0	0.05	0.485	0.633	0.719	0.806	0.877	0.88	0.882	0.885	0.887
Z_1=0.3	0.04	0.475	0.608	0.665	0.739	0.814	0.817	0.82	0.823	0.827
Z_1=0.6	0.004	0.199	0.258	0.312	0.357	0.388	0.406	0.429	0.5	0.5
Z_1=0.9	0.0	0.081	0.104	0.144	0.144	0.169	0.174	0.191	0.215	0.226

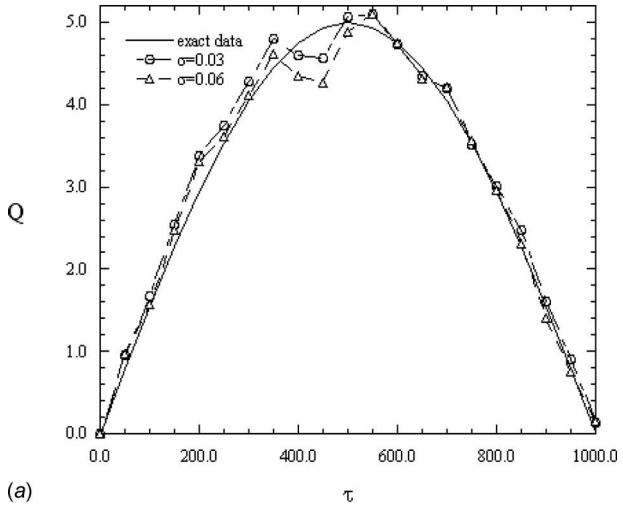

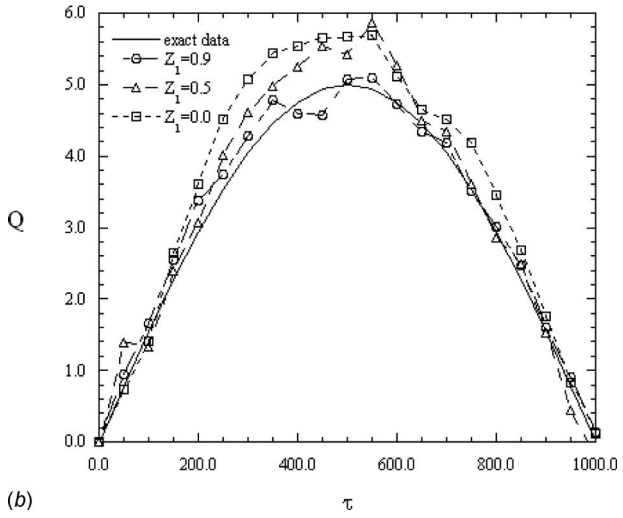

Fig. 5 Comparison of the exact result and inverse results for the Case 2 heat flux profile: (*a*) $\sigma=0.03$ and $\sigma=0.06$ ($Z_1=0.9$) and (*b*) $Z_1=0.0$, $Z_1=0.5$, and $Z_1=0.9$ ($\sigma=0.03$)

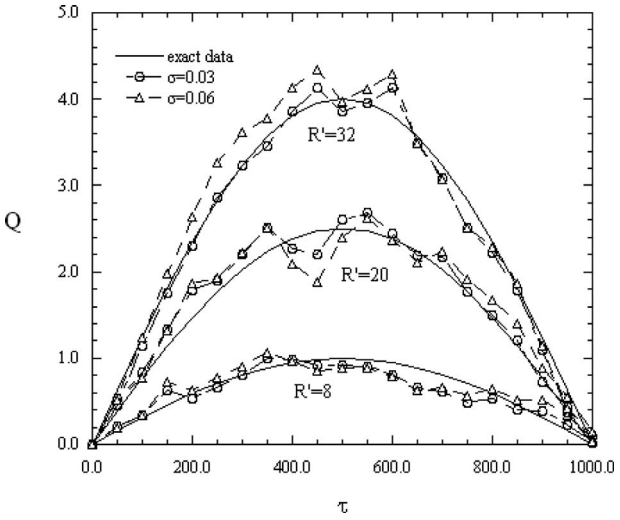

Fig. 7 Comparison of the exact result and inverse results ($\sigma=0.03$ and $\sigma=0.06$) for the Case 3 heat flux profile ($Z_1=0.9$)

of Case 3 and compared with the exact data; the sensor location is $Z_1=0.9$. As shown, the heat flux considered in this example is both time- and space-dependent. In general, it can be seen that the absolute value of the heat flux increases with an increasing value of R'. Finally, it is noted that for a given value of R', the accuracy of the estimated results improves as the measurement error reduces. Figure 8 shows the variation of the absolute average error with the sensor location as a function of the measurement error. As in previous examples, it can be seen that the accuracy of the estimated results improves as the sensor is moved toward the unknown boundary surface or as the measurement error is reduced. Table 2 summarizes the variation of the absolute average error as a function of both the measurement error and the sensor location. The results show that the accuracy of the estimated results reduces when the sensor is positioned closer to the lower wall. For example, given a constant measurement error of $\sigma=0.09$, the estimation errors corresponding to sensor locations of $Z_1=0.0$, 0.3, 0.6, and 0.9 are found to be 1.055, 1.017, 0.436, and 0.246, re-

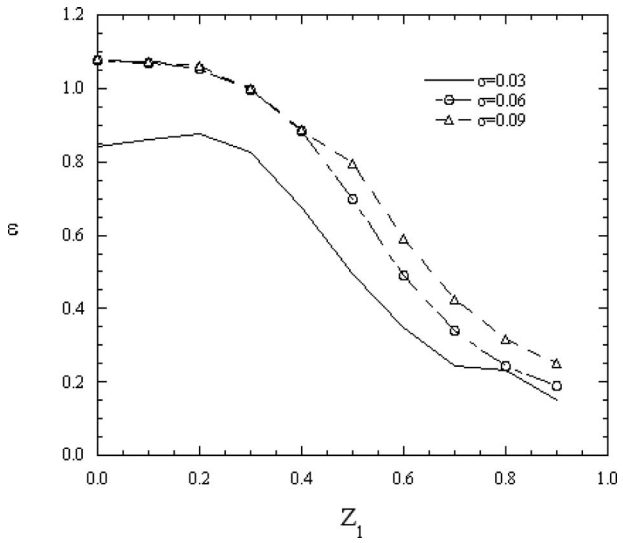

Fig. 6 Variation of the absolute average error with the sensor location as a function of the measurement error for the Case 2 heat flux profile

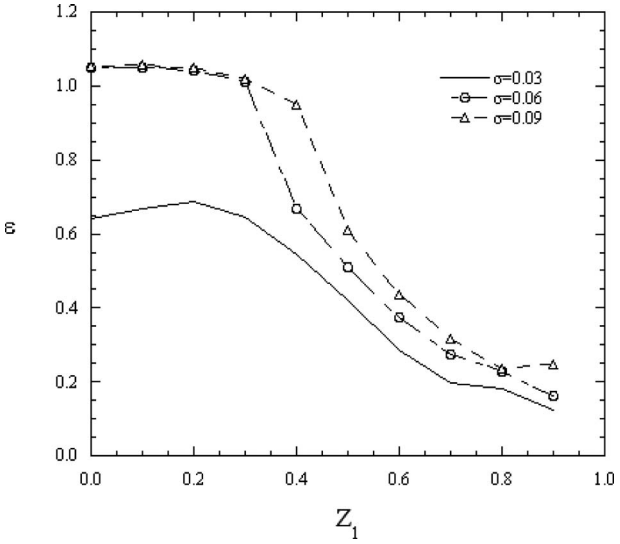

Fig. 8 Variation of the absolute average error with the sensor location as a function of the measurement error for the Case 3 heat flux profile

Table 2 The absolute average errors at different σ and Z_1 for the wall heating condition of Case 3

Z_1	0.0	0.1	0.2	0.3	0.4	0.5	0.6	0.7	0.8	0.9
σ=0.0	0.071	0.07	0.068	0.034	0.028	0.008	0.004	0.001	0.0	0.0
σ=0.03	0.642	0.668	0.687	0.645	0.544	0.422	0.285	0.195	0.181	0.125
σ=0.06	1.049	1.049	1.043	1.01	0.669	0.511	0.373	0.273	0.227	0.162
σ=0.09	1.055	1.056	1.05	1.017	0.948	0.611	0.436	0.317	0.234	0.246

spectively. However, it is apparent that the effect of the sensor location on the accuracy of the estimated results becomes less pronounced as the measurement error reduces.

In general, the results presented in this section of the paper confirm the ability of the proposed inverse solution scheme to estimate surface heat flux profiles of various forms given knowledge of the corresponding temperature distribution within the fluid field. Overall, the results demonstrate that the accuracy of the estimated solutions is enhanced as the temperature sensors are moved toward the unknown boundary surface or the precision of the measured temperature data is improved.

4 Conclusions

This study has presented an inverse scheme based on the conjugate gradient method to estimate the space- and time-dependent wall heat flux in the problem of unsteady conjugated forced convection between two parallel corotating disks. The validity of the proposed approach has been demonstrated by considering three different heat flux profiles. In general, the results have shown that the solution scheme yields satisfactory results for all three profiles. It has also been shown that the accuracy of the estimated results can be enhanced by suppressing the error in the measurement data or by locating the temperature sensors closer to the unknown boundary surface.

Acknowledgment

The financial support provided to this study by the National Science Council of the Republic of China under Contract No. NSC 96-2221-E-269-007 is gratefully acknowledged.

Nomenclature

A = dimensionless thermal diffusivity
d = direction of descent
f = estimated result with measurement errors
f_0 = exact result
h = heat transfer coefficient
J = objective function
K = dimensionless thermal conductivity
k = thermal conductivity
M = number of the measured data in the R direction
N = number of the measured data in the τ direction
n_t = number of temporal steps
P', p' = dimensionless and dimensional pressure departures
Pe = Peclet number
Q = dimensionless wall heat flux
q_w = wall heat flux
q_{ref} = reference heat flux
R, r = dimensionless and dimensional radial coordinates
R = dimensionless relative radial position
$R_{\text{in}}, r_{\text{in}}$ = dimensionless and dimensional radius openings
Re = Reynolds number
Ro = rotation number
s = disk spacing
T = temperature
T_{in} = inlet temperature
t = time
U, V, W = dimensionless velocity
u_{in} = inlet velocity
u, v, w = velocity
Z_1 = Z-coordinate position of temperature sensors
Θ = measured dimensionless temperature data

Greek Symbols

α = thermal diffusivity
β = step size
δ = disk wall thickness
ε = absolute average error
γ = conjugate coefficient
Ω = angular speed of corotating disks
φ = specified positive number
λ = dimensionless disk wall thickness
ν = kinematic viscosity
θ = dimensionless temperature
σ = standard deviation
τ = dimensionless time
ζ = random variable

Superscript

p = pth iteration

Subscripts

f = fluid
w = wall

References

[1] Beck, J. V., Blackwell, B., and Clair, C. R., 1985, *Inverse Heat Conduction: Ill-Posed Problems*, Wiley, New York.
[2] Alifanov, O. M., 1994, *Inverse Heat Transfer Problems*, Springer-Verlag, New York.
[3] Kurpisz, K., and Nowak, A. J., 1995, *Inverse Thermal Problems*, Computational Mechanics, Southampton.
[4] Ozisik, M. N., and Orlande, H. R. B., 2000, *Inverse Heat Transfer*, Taylor & Francis, New York.
[5] Moutsoglou, A., 1990, "Solution of an Elliptic Inverse Convection Problem Using a Whole Domain Regularization Technique," J. Thermophys. Heat Transfer, **4**(3), pp. 341–349.
[6] Colaco, M. J., and Orlande, H. R. B., 2001, "Inverse Forced Convection Problem of Simultaneous Estimation of Two Boundary Heat Fluxes in Irregularly Shaped Channels," Numer. Heat Transfer, Part A, **39**(7), pp. 737–760.
[7] Huang, C. H., and Ozisik, M. N., 1992, "Inverse Problem of Determining Unknown Wall Heat Flux in Laminar Flow Through a Parallel Plate Duct," Numer. Heat Transfer, Part A, **21**(1), pp. 55–70.
[8] Liu, F. B., and Ozisik, M. N., 1996, "Inverse Analysis of Transient Turbulent Forced Convection Inside Parallel−Plate Ducts," Int. J. Heat Mass Transfer, **39**(12), pp. 2615–2618.
[9] Raghunath, R., 1993, "Determining Entrance Conditions From Downstream Measurements," Int. Commun. Heat Mass Transfer, **20**, pp. 173–183.
[10] Bokar, J. C., and Ozisik, M. N., 1995, "An Inverse Analysis for Estimating the Time-Varying Inlet Temperature in Laminar Flow Inside a Parallel Plate Duct," Int. J. Heat Mass Transfer, **38**, pp. 39–45.
[11] Liu, F. B., and Ozisik, M. N., 1996, "Estimation of Inlet Temperature Profile in Laminar Duct Flow," Inverse Probl. Eng., **3**, pp. 131–143.
[12] Machado, H. A., and Orlande, H. R. B., 1997, "Inverse Analysis for Estimating the Timewise and Spacewise Variation of the Heat Flux in a Parallel Plate Channel," Int. J. Numer. Methods Heat Fluid Flow, **7**, pp. 696–710.
[13] Park, H. M., and Lee, J. H., 1998, "A Method of Solving Inverse Convection Problem by Means of Mode Reduction," Chem. Eng. Sci., **53**, pp. 1731–1744.
[14] Fic, A., 2004, "A Study of the Steady-State Inverse Heat Transfer Problem of Estimating the Boundary Velocity," Numer. Heat Transfer, Part A, **45**(2), pp. 153–170.

[15] Li, H. Y., and Yan, W. M., 1999, "Estimation of Space and Time Dependent Wall Heat Flux in an Inverse Convection Problem," J. Thermophys. Heat Transfer, **13**(3), pp. 394–396.
[16] Li, H. Y., and Yan, W. M., 2003, "Identification of Wall Heat Flux for Turbulent Forced Convection by Inverse Analysis," Int. J. Heat Mass Transfer, **46**, pp. 1041–1048.
[17] Li, H. Y., and Yan, W. M., 2000, "Inverse Convection Problem for Determining Wall Heat Flux in Annular Duct Flow," ASME J. Heat Transfer, **122**(3), pp. 460–464.
[18] Chen, C. K., Wu, L. W., and Yang, Y. T., 2006, "Comparison of Whole-Domain and Sequential Algorithms for Function Specification Method in the Inverse Heat Transfer Problem of Laminar Convective Pipe Flow," Numer. Heat Transfer, Part A, **50**(10), pp. 927–947.
[19] Chen, C. K., Wu, L. W., and Yang, Y. T., 2008, "Proposed Modification to Whole Domain Function Specification Method to Improve Accuracy of Its Estimations," ASME J. Heat Transfer, **130**, pp. 051702.
[20] Attia, H. A., 2003, "Unsteady Flow of a Non-Newtonian Fluid Above a Rotating Disk With Heat Transfer," Int. J. Heat Mass Transfer, **46**, pp. 2695–2700.
[21] Seghir-Ouali, S., Saury, D., Harmand, S., Phillipart, O., and Laloy, D., 2006, "Convective Heat Transfer Inside a Rotating Cylinder With an Axial Air Flow," Int. J. Therm. Sci., **45**, pp. 1166–1178.
[22] Siddquiddi, A. M., Rana, M. A., and Ahmed, N., 2008, "Effects of Hall Current and Heat Transfer on MHD Flow of a Burger's Fluid Due to a Pull of Eccentric Rotating Disks," Commun. Nonlinear Sci. Numer. Simul., **13**, pp. 1554–1570.
[23] Aus der Wiesche, S., 2007, "Heat Transfer From a Rotating Disk in a Parallel Air Crossflow," Int. J. Therm. Sci., **46**, pp. 745–754.
[24] Lee, K. T., and Yan, W. M., 1994, "Numerical Study of Transient Conjugated Mixed Convection in a Vertical Pipe," Numer. Heat Transfer, **26**, pp. 161–179.
[25] Yan, W. M., and Lee, K. T., 1995, "Unsteady Conjugated Mixed Convection in a Vertical Channel," ASME J. Heat Transfer, **117**, pp. 234–238.
[26] Yan, W. M., and Lee, K. T., 1996, "Unsteady Conjugated Mixed Convection Flow and Heat Transfer Between Two Co-Rotating Discs," Int. J. Heat Mass Transfer, **40**, pp. 2975–2988.
[27] Luna, N., Méndez, F., and Mar, E., 2003, "Transient Analysis of the Conjugated Heat Transfer in Circular Ducts With a Power Law Fluid," J. Non-Newtonian Fluid Mech., **111**, pp. 69–85.
[28] Indinger, T., and Shevchuk, I. V., 2004, "Transient Laminar Conjugate Heat Transfer of a Rotating Disk: Theory and Numerical Simulations," Int. J. Heat Mass Transfer, **47**, pp. 3577–3581.
[29] Ozar, B., Cetegen, B. M., and Faghri, A., 2004, "Experiments on Heat Transfer in a Thin Liquid Film Flowing Over a Rotating Disk," ASME J. Heat Transfer, **126**, pp. 184–192.
[30] Basu, S., and Cetegen, B. M., 2006, "Analysis of Hydrodynamics and Heat Transfer in a Thin Liquid Film Flowing Over a Rotating Disk by the Integral Method," ASME J. Heat Transfer, **128**, pp. 217–225.
[31] Basu, S., and Cetegen, B. M., 2007, "Effect of Hydraulic Jump on Hydrodynamics and Heat Transfer in a Thin Liquid Film Flowing Over a Rotating Disk Analyzed by Integral Method," ASME J. Heat Transfer, **129**, pp. 657–663.
[32] Shevchuk, I. V., 2006, "Unsteady Conjugate Laminar Heat Transfer of a Rotating Non-Uniformly Heated Disk: Application to the Transient Experimental Technique," Int. J. Heat Mass Transfer, **49**, pp. 3530–3537.
[33] Lallave, J. C., Rahman, M. M., and Kumar, A., 2007, "Numerical Analysis of Heat Transfer on a Rotating Disk Surface Under Confined Liquid Jet Impingement," Int. J. Heat Fluid Flow, **28**, pp. 720–734.
[34] Sladek, J., Sladek, V., and Hon, Y. C., 2006, "Inverse Heat Conduction Problems by Meshless Local Petrov–Galerkin Method," Eng. Anal. Boundary Elem., **30**, pp. 250–261.
[35] Yan, W. M., Tsay, Y. L., and Lin, T. F., 1989, "Transient Conjugated Heat Transfer in Laminar Pipe Flows," Int. J. Heat Mass Transfer, **32**, pp. 775–777.
[36] Patankar, S. V., 1980, *Numerical Heat Transfer and Fluid Flow*, Hemisphere, Washington, DC.
[37] Hestenes, M. R., 1980, *Conjugate Direction Methods in Optimization*, Springer-Verlag, New York, Chap. 4.
[38] Alifanov, O. M., 1974, "Solution of an Inverse Problem of Heat Conduction by Iteration Methods," J. Eng. Phys., **26**(4), pp. 471–476.
[39] 1987, User's Manual, Math Library Version 1.0, IMSL Library Edition 10.0, IMSL, Houston, TX.